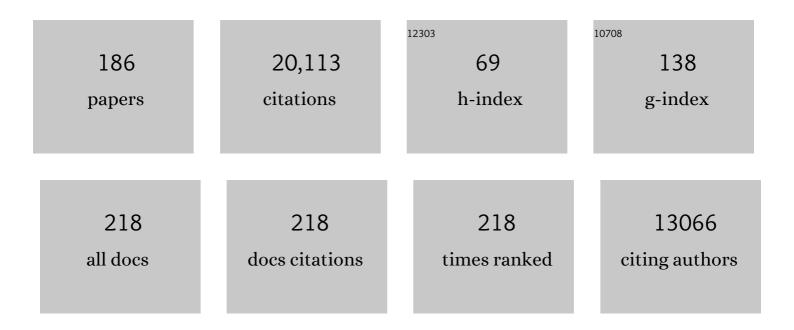
Qihao Weng

List of Publications by Year in descending order

Source: https://exaly.com/author-pdf/3591710/publications.pdf Version: 2024-02-01



#	Article	IF	CITATIONS
1	A survey of image classification methods and techniques for improving classification performance. International Journal of Remote Sensing, 2007, 28, 823-870.	1.3	2,334
2	Estimation of land surface temperature–vegetation abundance relationship for urban heat island studies. Remote Sensing of Environment, 2004, 89, 467-483.	4.6	1,760
3	Per-pixel vs. object-based classification of urban land cover extraction using high spatial resolution imagery. Remote Sensing of Environment, 2011, 115, 1145-1161.	4.6	1,040
4	Thermal infrared remote sensing for urban climate and environmental studies: Methods, applications, and trends. ISPRS Journal of Photogrammetry and Remote Sensing, 2009, 64, 335-344.	4.9	883
5	Remote sensing of impervious surfaces in the urban areas: Requirements, methods, and trends. Remote Sensing of Environment, 2012, 117, 34-49.	4.6	841
6	Land use change analysis in the Zhujiang Delta of China using satellite remote sensing, GIS and stochastic modelling. Journal of Environmental Management, 2002, 64, 273-284.	3.8	655
7	Use of impervious surface in urban land-use classification. Remote Sensing of Environment, 2006, 102, 146-160.	4.6	542
8	Generating daily land surface temperature at Landsat resolution by fusing Landsat and MODIS data. Remote Sensing of Environment, 2014, 145, 55-67.	4.6	399
9	Spatial–temporal dynamics of land surface temperature in relation to fractional vegetation cover and land use/cover in the Tabriz urban area, Iran. Remote Sensing of Environment, 2009, 113, 2606-2617.	4.6	359
10	A time series analysis of urbanization induced land use and land cover change and its impact on land surface temperature with Landsat imagery. Remote Sensing of Environment, 2016, 175, 205-214.	4.6	357
11	Modeling Urban Growth Effects on Surface Runoff with the Integration of Remote Sensing and GIS. Environmental Management, 2001, 28, 737-748.	1.2	304
12	Spectral Mixture Analysis of the Urban Landscape in Indianapolis with Landsat ETM+ Imagery. Photogrammetric Engineering and Remote Sensing, 2004, 70, 1053-1062.	0.3	299
13	Estimating impervious surfaces from medium spatial resolution imagery using the self-organizing map and multi-layer perceptron neural networks. Remote Sensing of Environment, 2009, 113, 2089-2102.	4.6	232
14	Geographic object-based image analysis (GEOBIA): emerging trends and future opportunities. GIScience and Remote Sensing, 2018, 55, 159-182.	2.4	205
15	A sub-pixel analysis of urbanization effect on land surface temperature and its interplay with impervious surface and vegetation coverage in Indianapolis, United States. International Journal of Applied Earth Observation and Geoinformation, 2008, 10, 68-83.	1.4	195
16	Fractal Analysis of Satellite-Detected Urban Heat Island Effect. Photogrammetric Engineering and Remote Sensing, 2003, 69, 555-566.	0.3	190
17	The impact of land use and land cover changes on land surface temperature in a karst area of China. Journal of Environmental Management, 2007, 85, 245-257.	3.8	189
18	A remote sensing?GIS evaluation of urban expansion and its impact on surface temperature in the Zhujiang Delta, China. International Journal of Remote Sensing, 2001, 22, 1999-2014.	1.3	183

#	Article	IF	CITATIONS
19	Remote Sensing Sensors and Applications in Environmental Resources Mapping and Modelling. Sensors, 2007, 7, 3209-3241.	2.1	181
20	A remote sensing–GIS evaluation of urban expansion and its impact on surface temperature in the Zhujiang Delta, China. International Journal of Remote Sensing, 2001, 22, 1999-2014.	1.3	175
21	Seasonal Variations of the Surface Urban Heat Island in a Semi-Arid City. Remote Sensing, 2016, 8, 352.	1.8	167
22	Managing the adverse thermal effects of urban development in a densely populated Chinese city. Journal of Environmental Management, 2004, 70, 145-156.	3.8	163
23	Assessing the effects of land use and land cover patterns on thermal conditions using landscape metrics in city of Indianapolis, United States. Urban Ecosystems, 2007, 10, 203-219.	1.1	160
24	Urban Classification Using Full Spectral Information of Landsat ETM+ Imagery in Marion County, Indiana. Photogrammetric Engineering and Remote Sensing, 2005, 71, 1275-1284.	0.3	158
25	Spectral mixture analysis of ASTER images for examining the relationship between urban thermal features and biophysical descriptors in Indianapolis, Indiana, USA. Remote Sensing of Environment, 2006, 104, 157-167.	4.6	157
26	Extraction of urban impervious surfaces from an IKONOS image. International Journal of Remote Sensing, 2009, 30, 1297-1311.	1.3	155
27	Measuring the quality of life in city of Indianapolis by integration of remote sensing and census data. International Journal of Remote Sensing, 2007, 28, 249-267.	1.3	148
28	Urban heat island monitoring and analysis using a non-parametric model: A case study of Indianapolis. ISPRS Journal of Photogrammetry and Remote Sensing, 2009, 64, 86-96.	4.9	144
29	Urban Air Pollution Patterns, Land Use, and Thermal Landscape: An Examination of the Linkage Using GIS. Environmental Monitoring and Assessment, 2006, 117, 463-489.	1.3	137
30	Simulating the impacts of future land use and climate changes on surface water quality in the Des Plaines River watershed, Chicago Metropolitan Statistical Area, Illinois. Science of the Total Environment, 2011, 409, 4387-4405.	3.9	129
31	Enhancing temporal resolution of satellite imagery for public health studies: A case study of West Nile Virus outbreak in Los Angeles in 2007. Remote Sensing of Environment, 2012, 117, 57-71.	4.6	129
32	Medium Spatial Resolution Satellite Imagery for Estimating and Mapping Urban Impervious Surfaces Using LSMA and ANN. IEEE Transactions on Geoscience and Remote Sensing, 2008, 46, 2397-2406.	2.7	127
33	Annual dynamics of impervious surface in the Pearl River Delta, China, from 1988 to 2013, using time series Landsat imagery. ISPRS Journal of Photogrammetry and Remote Sensing, 2016, 113, 86-96.	4.9	126
34	High-Resolution Satellite Mapping of Fine Particulates Based on Geographically Weighted Regression. IEEE Geoscience and Remote Sensing Letters, 2016, 13, 495-499.	1.4	126
35	The Role of Vegetation in Mitigating Urban Land Surface Temperatures: A Case Study of Munich, Germany during the Warm Season. Sustainability, 2015, 7, 4689-4706.	1.6	125
36	Seasonal variations in the relationship between landscape pattern and land surface temperature in Indianapolis, USA. Environmental Monitoring and Assessment, 2008, 144, 199-219.	1.3	122

#	Article	IF	CITATIONS
37	Extracting impervious surfaces from medium spatial resolution multispectral and hyperspectral imagery: a comparison. International Journal of Remote Sensing, 2008, 29, 3209-3232.	1.3	121
38	Land Use and Land Cover Change in Guangzhou, China, from 1998 to 2003, Based on Landsat TM /ETM+ Imagery. Sensors, 2007, 7, 1323-1342.	2.1	116
39	Developing a new cross-sensor calibration model for DMSP-OLS and Suomi-NPP VIIRS night-light imageries. ISPRS Journal of Photogrammetry and Remote Sensing, 2019, 153, 36-47.	4.9	114
40	Modeling Urban Heat Islands and Their Relationship With Impervious Surface and Vegetation Abundance by Using ASTER Images. IEEE Transactions on Geoscience and Remote Sensing, 2011, 49, 4080-4089.	2.7	113
41	A new source of multi-spectral high spatial resolution night-time light imagery—JL1-3B. Remote Sensing of Environment, 2018, 215, 300-312.	4.6	113
42	Assessing Surface Water Quality and Its Relation with Urban Land Cover Changes in the Lake Calumet Area, Greater Chicago. Environmental Management, 2010, 45, 1096-1111.	1.2	112
43	Modeling annual parameters of clear-sky land surface temperature variations and evaluating the impact of cloud cover using time series of Landsat TIR data. Remote Sensing of Environment, 2014, 140, 267-278.	4.6	111
44	Land Surface Temperature Variation and Major Factors in Beijing, China. Photogrammetric Engineering and Remote Sensing, 2008, 74, 451-461.	0.3	110
45	Identification and analysis of urban surface temperature patterns in Greater Athens, Greece, using MODIS imagery. Remote Sensing of Environment, 2011, 115, 3080-3090.	4.6	110
46	Urban Surface Biophysical Descriptors and Land Surface Temperature Variations. Photogrammetric Engineering and Remote Sensing, 2006, 72, 1275-1286.	0.3	106
47	Residential population estimation using a remote sensing derived impervious surface approach. International Journal of Remote Sensing, 2006, 27, 3553-3570.	1.3	106
48	Bias-corrected rational polynomial coefficients for high accuracy geo-positioning of QuickBird stereo imagery. ISPRS Journal of Photogrammetry and Remote Sensing, 2010, 65, 218-226.	4.9	106
49	Scaling Effect on the Relationship between Landscape Pattern and Land Surface Temperature. Photogrammetric Engineering and Remote Sensing, 2009, 75, 291-304.	0.3	103
50	Updating urban extents with nighttime light imagery by using an object-based thresholding method. Remote Sensing of Environment, 2016, 187, 1-13.	4.6	101
51	An evaluation of monthly impervious surface dynamics by fusing Landsat and MODIS time series in the Pearl River Delta, China, from 2000 to 2015. Remote Sensing of Environment, 2017, 201, 99-114.	4.6	100
52	A Review on Remote Sensing of Urban Heat and Cool Islands. Land, 2017, 6, 38.	1.2	100
53	Collective Sensing: Integrating Geospatial Technologies to Understand Urban Systems—An Overview. Remote Sensing, 2011, 3, 1743-1776.	1.8	99
54	Detecting urban-scale dynamics of electricity consumption at Chinese cities using time-series DMSP-OLS (Defense Meteorological Satellite Program-Operational Linescan System) nighttime light imageries. Energy, 2016, 100, 177-189.	4.5	96

#	Article	IF	CITATIONS
55	Impervious surface area extraction from IKONOS imagery using an object-based fuzzy method. Geocarto International, 2011, 26, 3-20.	1.7	91
56	Using Landsat ETM + Imagery to Measure Population Density in Indianapolis, Indiana, USA. Photogrammetric Engineering and Remote Sensing, 2005, 71, 947-958.	0.3	90
57	Estimation of the relationship between remotely sensed anthropogenic heat discharge and building energy use. ISPRS Journal of Photogrammetry and Remote Sensing, 2012, 67, 65-72.	4.9	90
58	Estimating impervious surfaces using linear spectral mixture analysis with multitemporal ASTER images. International Journal of Remote Sensing, 2009, 30, 4807-4830.	1.3	88
59	Mapping impervious surface expansion using medium-resolution satellite image time series: a case study in the Yangtze River Delta, China. International Journal of Remote Sensing, 2012, 33, 7609-7628.	1.3	88
60	Assessing the Impacts of Urbanization-Associated Land Use/Cover Change on Land Surface Temperature and Surface Moisture: A Case Study in the Midwestern United States. Remote Sensing, 2015, 7, 4880-4898.	1.8	87
61	A large-scale change monitoring of wetlands using time series Landsat imagery on Google Earth Engine: a case study in Newfoundland. GIScience and Remote Sensing, 2020, 57, 1102-1124.	2.4	87
62	The Spatial Variations of Urban Land Surface Temperatures: Pertinent Factors, Zoning Effect, and Seasonal Variability. IEEE Journal of Selected Topics in Applied Earth Observations and Remote Sensing, 2008, 1, 154-166.	2.3	83
63	A Geographically Weighted Regression Analysis of the Underlying Factors Related to the Surface Urban Heat Island Phenomenon. Remote Sensing, 2018, 10, 1428.	1.8	83
64	An object-based approach to delineate wetlands across landscapes of varied disturbance with high spatial resolution satellite imagery. ISPRS Journal of Photogrammetry and Remote Sensing, 2015, 109, 30-46.	4.9	80
65	Estimating Composite Curve Number Using an Improved SCS-CN Method with Remotely Sensed Variables in Guangzhou, China. Remote Sensing, 2013, 5, 1425-1438.	1.8	78
66	Assessing Urban Environmental Quality Change of Indianapolis, United States, by the Remote Sensing and GIS Integration. IEEE Journal of Selected Topics in Applied Earth Observations and Remote Sensing, 2011, 4, 43-55.	2.3	77
67	Variability in annual temperature cycle in the urban areas of the United States as revealed by MODIS imagery. ISPRS Journal of Photogrammetry and Remote Sensing, 2018, 146, 65-73.	4.9	77
68	Modeling diurnal land temperature cycles over Los Angeles using downscaled GOES imagery. ISPRS Journal of Photogrammetry and Remote Sensing, 2014, 97, 78-88.	4.9	75
69	Temporal variations of artificial nighttime lights and their implications for urbanization in the conterminous United States, 2013–2017. Remote Sensing of Environment, 2019, 225, 160-174.	4.6	71
70	Characterizing the spatial pattern of annual urban growth by using time series Landsat imagery. Science of the Total Environment, 2019, 666, 274-284.	3.9	70
71	Statistical analysis of surface urban heat island intensity variations: A case study of Babol city, Iran. GIScience and Remote Sensing, 2019, 56, 576-604.	2.4	70
72	Spatioâ€ŧemporal modelling and analysis of urban heat islands by using Landsat TM and ETM+ imagery. International Journal of Remote Sensing, 2009, 30, 3531-3548.	1.3	69

#	Article	IF	CITATIONS
73	Monitoring Urban Dynamics in the Southeast U.S.A. Using Time-Series DMSP/OLS Nightlight Imagery. Remote Sensing, 2016, 8, 578.	1.8	69
74	Spatiotemporally enhancing time-series DMSP/OLS nighttime light imagery for assessing large-scale urban dynamics. ISPRS Journal of Photogrammetry and Remote Sensing, 2017, 128, 1-15.	4.9	69
75	Integrating UAV optical imagery and LiDAR data for assessing the spatial relationship between mangrove and inundation across a subtropical estuarine wetland. ISPRS Journal of Photogrammetry and Remote Sensing, 2019, 149, 146-156.	4.9	68
76	World energy consumption pattern as revealed by DMSP-OLS nighttime light imagery. GIScience and Remote Sensing, 2016, 53, 265-282.	2.4	67
77	Consistent land surface temperature data generation from irregularly spaced Landsat imagery. Remote Sensing of Environment, 2016, 184, 175-187.	4.6	62
78	Surface anthropogenic heat islands in six megacities: An assessment based on a triple-source surface energy balance model. Remote Sensing of Environment, 2020, 242, 111751.	4.6	61
79	Downscaling Geostationary Land Surface Temperature Imagery for Urban Analysis. IEEE Geoscience and Remote Sensing Letters, 2013, 10, 1253-1257.	1.4	60
80	Modeling of Anthropogenic Heat Flux Using HJ-1B Chinese Small Satellite Image: A Study of Heterogeneous Urbanized Areas in Hong Kong. IEEE Geoscience and Remote Sensing Letters, 2015, 12, 1466-1470.	1.4	60
81	Estimation of hourly and daily evapotranspiration and soil moisture using downscaled LST over various urban surfaces. GIScience and Remote Sensing, 2017, 54, 95-117.	2.4	60
82	Google Earth Engine for large-scale land use and land cover mapping: an object-based classification approach using spectral, textural and topographical factors. GIScience and Remote Sensing, 2021, 58, 914-928.	2.4	57
83	Spatiotemporal Variation of Surface Urban Heat Islands in Relation to Land Cover Composition and Configuration: A Multi-Scale Case Study of Xi'an, China. Remote Sensing, 2020, 12, 2713.	1.8	56
84	Assessment of urban environmental change using multi-source remote sensing time series (2000–2016): A comparative analysis in selected megacities in Eurasia. Science of the Total Environment, 2019, 684, 567-577.	3.9	55
85	Normalizing land surface temperature for environmental parameters in mountainous and urban areas of a cold semi-arid climate. Science of the Total Environment, 2019, 650, 515-529.	3.9	55
86	Characterizing urban land changes of 30 global megacities using nighttime light time series stacks. ISPRS Journal of Photogrammetry and Remote Sensing, 2021, 173, 10-23.	4.9	55
87	Urban Land Cover Classification With Airborne Hyperspectral Data: What Features to Use?. IEEE Journal of Selected Topics in Applied Earth Observations and Remote Sensing, 2014, 7, 3998-4009.	2.3	54
88	Landscape as a continuum: an examination of the urban landscape structures and dynamics of Indianapolis City, 1991–2000, by using satellite images. International Journal of Remote Sensing, 2009, 30, 2547-2577.	1.3	51
89	Landscape metrics for analysing urbanization-induced land use and land cover changes. Geocarto International, 2013, 28, 582-593.	1.7	51
90	Population Estimation of Urban Residential Communities Using Remotely Sensed Morphologic Data. IEEE Geoscience and Remote Sensing Letters, 2015, 12, 1111-1115.	1.4	51

#	Article	IF	CITATIONS
91	Responses of urban heat island in Atlanta to different land-use scenarios. Theoretical and Applied Climatology, 2018, 133, 123-135.	1.3	51
92	A physical model-based method for retrieving urban land surface temperatures under cloudy conditions. Remote Sensing of Environment, 2019, 230, 111191.	4.6	51
93	An assessment of urbanization sustainability in China between 1990 and 2015 using land use efficiency indicators. Npj Urban Sustainability, 2021, 1, .	3.7	50
94	An Automated Method to Parameterize Segmentation Scale by Enhancing Intrasegment Homogeneity and Intersegment Heterogeneity. IEEE Geoscience and Remote Sensing Letters, 2015, 12, 1282-1286.	1.4	48
95	A remote sensing–GIS evaluation of urban expansion and its impact on surface temperature in the Zhujiang Delta, China. International Journal of Remote Sensing, 2001, 22, 1999-2014.	1.3	47
96	Multiscale Analysis of Census-Based Land Surface Temperature Variations and Determinants in Indianapolis, United States. Journal of the Urban Planning and Development Division, ASCE, 2008, 134, 129-139.	0.8	46
97	Tidal and Meteorological Influences on the Growth of Invasive Spartina alterniflora: Evidence from UAV Remote Sensing. Remote Sensing, 2019, 11, 1208.	1.8	46
98	The Second Generation Canadian Wetland Inventory Map at 10 Meters Resolution Using Google Earth Engine. Canadian Journal of Remote Sensing, 2020, 46, 360-375.	1.1	46
99	Use of Local Climate Zones to investigate surface urban heat islands in Texas. GIScience and Remote Sensing, 2020, 57, 1083-1101.	2.4	46
100	An automated deep learning convolutional neural network algorithm applied for soil salinity distribution mapping in Lake Urmia, Iran. Science of the Total Environment, 2021, 778, 146253.	3.9	44
101	Spatio-temporal analysis of the relationship between WNV dissemination and environmental variables in Indianapolis, USA. International Journal of Health Geographics, 2008, 7, 66.	1.2	43
102	Local Impacts of the Post-Mao Development Strategy: The Case of the Zhujiang Delta, Southern China. International Journal of Urban and Regional Research, 1998, 22, 425-442.	1.2	42
103	Assessing Intra-Urban Surface Energy Fluxes Using Remotely Sensed ASTER Imagery and Routine Meteorological Data: A Case Study in Indianapolis, U.S.A IEEE Journal of Selected Topics in Applied Earth Observations and Remote Sensing, 2014, 7, 4046-4057.	2.3	42
104	Remotely Sensed Urban Surface Ecological Index (RSUSEI): An Analytical Framework for Assessing the Surface Ecological Status in Urban Environments. Remote Sensing, 2020, 12, 2029.	1.8	41
105	A historical perspective of river basin management in the Pearl River Delta of China. Journal of Environmental Management, 2007, 85, 1048-1062.	3.8	40
106	An examination of the effect of landscape pattern, land surface temperature, and socioeconomic conditions on WNV dissemination in Chicago. Environmental Monitoring and Assessment, 2009, 159, 143-161.	1.3	40
107	Modeling the spatial variation of urban land surface temperature in relation to environmental and anthropogenic factors: a case study of Tehran, Iran. GIScience and Remote Sensing, 2020, 57, 483-496.	2.4	40
108	High spatial- and temporal-resolution anthropogenic heat discharge estimation in Los Angeles County, California. Journal of Environmental Management, 2018, 206, 1274-1286.	3.8	39

#	Article	IF	CITATIONS
109	Modeling outdoor thermal comfort using satellite imagery: A principle component analysis-based approach. Ecological Indicators, 2020, 117, 106555.	2.6	38
110	Quantifying Uncertainty of Digital Elevation Models Derived from Topographic Maps. , 2002, , 403-418.		37
111	Characterizing the 3-D urban morphology transformation to understand urban-form dynamics: A case study of Austin, Texas, USA. Landscape and Urban Planning, 2020, 203, 103881.	3.4	36
112	Exploring diurnal cycles of surface urban heat island intensity in Boston with land surface temperature data derived from GOES-R geostationary satellites. Science of the Total Environment, 2021, 763, 144224.	3.9	36
113	Monitoring Urban Clusters Expansion in the Middle Reaches of the Yangtze River, China, Using Time-Series Nighttime Light Images. Remote Sensing, 2017, 9, 1007.	1.8	35
114	Application of airborne remote sensing data on mapping local climate zones: Cases of three metropolitan areas of Texas, U.S Computers, Environment and Urban Systems, 2019, 74, 175-193.	3.3	35
115	Improving Urban Impervious Surface Mapping by Linear Spectral Mixture Analysis and Using Spectral Indices. Canadian Journal of Remote Sensing, 2015, 41, 577-586.	1.1	34
116	Evaluation of ASTER-Like Daily Land Surface Temperature by Fusing ASTER and MODIS Data during the HiWATER-MUSOEXE. Remote Sensing, 2016, 8, 75.	1.8	33
117	A Hybrid Approach for Three-Dimensional Building Reconstruction in Indianapolis from LiDAR Data. Remote Sensing, 2017, 9, 310.	1.8	33
118	A PCA–OLS Model for Assessing the Impact of Surface Biophysical Parameters on Land Surface Temperature Variations. Remote Sensing, 2019, 11, 2094.	1.8	33
119	Impact of temporal compositing on nighttime light data and its applications. Remote Sensing of Environment, 2022, 274, 113016.	4.6	29
120	Modeling the effect of climate change on building energy demand in Los Angeles county by using a GIS-based high spatial- and temporal-resolution approach. Energy, 2019, 176, 641-655.	4.5	28
121	Application of Association Rule Mining for Exploring the Relationship between Urban Land Surface Temperature and Biophysical/Social Parameters. Photogrammetric Engineering and Remote Sensing, 2009, 75, 385-396.	0.3	27
122	Combinational shadow index for building shadow extraction in urban areas from Sentinel-2A MSI imagery. International Journal of Applied Earth Observation and Geoinformation, 2019, 78, 53-65.	1.4	27
123	Modeling the Effect of Green Roof Systems and Photovoltaic Panels for Building Energy Savings to Mitigate Climate Change. Remote Sensing, 2020, 12, 2402.	1.8	27
124	Spatial Analysis of Urban Growth Impacts on Vegetative Greenness with Landsat TM Data. Geocarto International, 2001, 16, 19-28.	1.7	26
125	Temporal Dynamics of Land Surface Temperature From Landsat TIR Time Series Images. IEEE Geoscience and Remote Sensing Letters, 2015, 12, 2175-2179.	1.4	24
126	Geometric Processing of QuickBird Stereo Imageries for Urban Land Use Mapping: A Case Study in Shanghai, China. IEEE Journal of Selected Topics in Applied Earth Observations and Remote Sensing, 2009, 2, 61-66.	2.3	23

#	Article	IF	CITATIONS
127	Model-Driven Reconstruction of 3-D Buildings Using LiDAR Data. IEEE Geoscience and Remote Sensing Letters, 2015, 12, 1541-1545.	1.4	23
128	Geographic incidence of human West Nile virus in northern Virginia, USA, in relation to incidence in birds and variations in urban environment. Science of the Total Environment, 2011, 409, 4235-4241.	3.9	22
129	Estimating impervious surfaces from medium spatial resolution imagery: a comparison between fuzzy classification and LSMA. International Journal of Remote Sensing, 2011, 32, 5645-5663.	1.3	22
130	An assessment of global electric power consumption using the Defense Meteorological Satellite Program-Operational Linescan System nighttime light imagery. Energy, 2019, 189, 116351.	4.5	22
131	Automatic mapping of urban green spaces using a geospatial neural network. GIScience and Remote Sensing, 2021, 58, 624-642.	2.4	22
132	Urban Sprawl and Changes in Land-Use Efficiency in the Beijing–Tianjin–Hebei Region, China from 2000 to 2020: A Spatiotemporal Analysis Using Earth Observation Data. Remote Sensing, 2021, 13, 2850.	1.8	22
133	An approach to evaluation of sustainability for Guangzhou's urban ecosystem. International Journal of Sustainable Development and World Ecology, 2003, 10, 69-81.	3.2	21
134	Scaling Effect of Fused ASTER-MODIS Land Surface Temperature in an Urban Environment. Sensors, 2018, 18, 4058.	2.1	21
135	Title is missing!. , 2000, 51, 191-202.		19
136	Analysis of surface radiation budget during the summer and winter in the metropolitan area of Beijing, China. Journal of Applied Remote Sensing, 2010, 4, 043513.	0.6	18
137	Investigating Spatiotemporal Patterns of Surface Urban Heat Islands in the Hangzhou Metropolitan Area, China, 2000–2015. Remote Sensing, 2019, 11, 1553.	1.8	18
138	Use of earth observation data for applications in public health. Geocarto International, 2014, 29, 3-16.	1.7	17
139	Downscaling GOES Land Surface Temperature for Assessing Heat Wave Health Risks. IEEE Geoscience and Remote Sensing Letters, 2015, 12, 1605-1609.	1.4	17
140	An Evaluation of Spatial Interpolation Accuracy of Elevation Data. , 2006, , 805-824.		16
141	Use of local climate zones to assess the spatiotemporal variations of urban vegetation phenology in Austin, Texas, USA. GIScience and Remote Sensing, 2022, 59, 393-409.	2.4	16
142	Correcting the Pixel Blooming Effect (PiBE) of DMSP-OLS nighttime light imagery. Remote Sensing of Environment, 2020, 240, 111707.	4.6	15
143	Fine-scale population estimation: how Landsat ETM+ imagery can improve population distribution mapping. Canadian Journal of Remote Sensing, 2010, 36, 155-165.	1.1	14
144	Multi-scale three-dimensional detection of urban buildings using aerial LiDAR data. GIScience and Remote Sensing, 2020, 57, 1125-1143.	2.4	14

#	Article	IF	CITATIONS
145	Thick Clouds Removing From Multitemporal Landsat Images Using Spatiotemporal Neural Networks. IEEE Transactions on Geoscience and Remote Sensing, 2022, 60, 1-14.	2.7	14
146	Satellite Remote Sensing of Urban Heat Islands: Current Practice and Prospects. , 2005, , 91-111.		13
147	Linking In Situ Photochemical Reflectance Index Measurements With Mangrove Carbon Dynamics in a Subtropical Coastal Wetland. Journal of Geophysical Research G: Biogeosciences, 2019, 124, 1714-1730.	1.3	13
148	Potential of Sunâ€Induced Chlorophyll Fluorescence for Indicating Mangrove Canopy Photosynthesis. Journal of Geophysical Research G: Biogeosciences, 2021, 126, e2020JG006159.	1.3	13
149	Introduction to the Issue on Remote Sensing of Human Settlements: Status and Challenges. IEEE Journal of Selected Topics in Applied Earth Observations and Remote Sensing, 2008, 1, 82-86.	2.3	12
150	Global 10-m impervious surface area mapping: A big earth data based extraction and updating approach. International Journal of Applied Earth Observation and Geoinformation, 2022, 109, 102800.	0.9	12
151	Homogeneity Distance Classification Algorithm (HDCA): A Novel Algorithm for Satellite Image Classification. Remote Sensing, 2019, 11, 546.	1.8	11
152	A Comparison between Sentinel-2 and Landsat 8 OLI Satellite Images for Soil Salinity Distribution Mapping Using a Deep Learning Convolutional Neural Network. Canadian Journal of Remote Sensing, 2022, 48, 452-468.	1.1	11
153	Estimation of impervious surfaces of Beijing, China, with spectral normalized images using linear spectral mixture analysis and artificial neural network. Geocarto International, 2010, 25, 231-253.	1.7	10
154	An evaluation of fractal characteristics of urban landscape in Indianapolis, USA, using multi-sensor satellite images. International Journal of Remote Sensing, 2013, 34, 804-823.	1.3	10
155	An Automatic Cloud Detection Neural Network for High-Resolution Remote Sensing Imagery With Cloud–Snow Coexistence. IEEE Geoscience and Remote Sensing Letters, 2022, 19, 1-5.	1.4	10
156	Post-War Urban Damage Mapping Using InSAR: The Case of Mosul City in Iraq. ISPRS International Journal of Geo-Information, 2021, 10, 140.	1.4	10
157	Learning-Based Methods for Detection and Monitoring of Shallow Flood-Affected Areas: Impact of Shallow-Flood Spreading on Vegetation Density. Canadian Journal of Remote Sensing, 2022, 48, 481-503.	1.1	10
158	Environmental Factors and Risk Areas of West Nile Virus in Southern California, 2007–2009. Environmental Modeling and Assessment, 2012, 17, 441-452.	1.2	8
159	Desert landform detection and mapping using a semi-automated object-based image analysis approach. Journal of Arid Environments, 2022, 199, 104721.	1.2	8
160	Operational earthquake-induced building damage assessment using CNN-based direct remote sensing change detection on superpixel level. International Journal of Applied Earth Observation and Geoinformation, 2022, 112, 102899.	0.9	8
161	LAND USE AND LAND COVER CHANGES IN CHINA UNDER REFORM AND GLOBALIZATION. Asian Geographer, 2003, 22, 1-3.	0.4	7
162	Distinctive roles of two- and three-dimensional urban structures in surface urban heat islands over the conterminous United States. Urban Climate, 2022, 44, 101230.	2.4	7

#	Article	IF	CITATIONS
163	A comparative study of NPP-VIIRS and DMSP-OLS nighttime light imagery for derivation of urban demographic metrics. , 2014, , .		6
164	An Analysis of the Discrepancies between MODIS and INSAT-3D LSTs in High Temperatures. Remote Sensing, 2017, 9, 347.	1.8	6
165	The relationship between the environmental change of the Zhujiang River Delta in Holocene and its cultural origins and propagation. Chinese Geographical Science, 1994, 4, 303-309.	1.2	5
166	GUANGZHOU'S GROWTH AND URBAN PLANNING, 1960–1997: AN ANALYSIS THROUGH REMOTE SENSING. Asian Geographer, 2003, 22, 77-92.	0.4	5
167	The Spatial Variability of Urban Land Surface Temperature. , 2007, , .		4
168	Foreword to the Issue on Remote Sensing of Regional Land Use and Land Cover. IEEE Journal of Selected Topics in Applied Earth Observations and Remote Sensing, 2009, 2, 50-53.	2.3	4
169	Clobal Urban Observation and Information: GEO's Effort to Address the Impacts of Human Settlements. Taylor & Francis Series in Remote Sensing Applications, 2014, , 15-34.	0.0	4
170	Characterizing Urban Landscape by Using Fractal-based Texture Information. Photogrammetric Engineering and Remote Sensing, 2018, 84, 695-710.	0.3	4
171	Estimating LST Using a Vegetation-Cover-Based Thermal Sharpening Technique. IEEE Geoscience and Remote Sensing Letters, 2013, 10, 1249-1252.	1.4	3
172	Assessing solar potential of commercial and residential buildings in Indianapolis using LiDAR and GIS modeling. , 2014, , .		3
173	Cenerating high spatial and temporal soil moisture data by disaggregation of SMAP product and its assessment in different land covers. GIScience and Remote Sensing, 2020, 57, 1046-1056.	2.4	3
174	What Is Special about Global Urban Remote Sensing?. Taylor & Francis Series in Remote Sensing Applications, 2014, , 1-12.	0.0	2
175	Essential Urban Variables from Satellite Observations: An Introduction. , 2018, , .		2
176	Estimation and seasonal monitoring of urban vegetation abundance based on remote sensing. Proceedings of SPIE, 2007, , .	0.8	1
177	Geographical applications of remote sensing. Geocarto International, 2013, 28, 561-561.	1.7	1
178	Estimating Tree Frontal Area in Urban Areas Using Terrestrial LiDAR Data. Remote Sensing, 2016, 8, 401.	1.8	1
179	Evaluation of the correlation between remotely sensing-based and GIS-based anthropogenic heat discharge in Los Angeles County, USA. , 2016, , .		1
180	Mapping Urban Impervious Surfaces from Medium and High Spatial Resolution Multispectral Imagery. Taylor & Francis Series in Remote Sensing Applications, 2007, , .	0.0	1

#	Article	IF	CITATIONS
181	Special Section Guest Editorial: Advances in Remote Sensing for Monitoring Global Environmental Changes. Journal of Applied Remote Sensing, 2012, 6, 061799.	0.6	0
182	Remote sensing detection of the spatial pattern of urban air pollution in Los Angeles. , 2014, , .		0
183	Temporally extrapolating object-based threshold for updating urban extents from nighttime light data. , 2016, , .		0
184	Remote sensors for and sensing of urban areas: Current state and next decade. , 2016, , .		0
185	Extracting Impervious Surface from Hyperspectral Imagery with Linear Spectral Mixture Analysis. Taylor & Francis Series in Remote Sensing Applications, 2007, , .	0.0	Ο
186	Using Remotely Sensed Impervious Surface Data to Estimate Population. Taylor & Francis Series in Remote Sensing Applications, 2007, , .	0.0	0